Preliminary non-intrusive geophysical electrical resistivity tomography surveys of a mock-up scale monitoring of EBS at URL Tournemire

Bruna de Carvalho Faria Lima Lopes[1*], Cédric Sachet[1], Philippe Sentenac[1], Vojtěch Beneš[2], Pierre Dick[3], Johan Bertrand[4] & Alessandro Tarantino[1]

[1]*Department of Civil and Environmental Engineering, University of Strathclyde, 65 Montrose Street Glasgow G1 1XJ, UK*

[2]*G Impuls, Přístavní 24, Praha 7, Prague 170 00, Czech Republic*

[3]*Institut de Radioprotection et de Sûreté Nucléaire, 31, Avenue de la Division Leclerc Fontenay-aux-Roses 92260, France*

[4]*Agence Nationale Pour La Gestion Des Déchets Radioactifs, 1-7, Rue Jean-Monnet Châtenay-Malabry cedex 92298, France*

**Corresponding author (email:* bruna.lopes@strath.ac.uk)

ORCiD: BCFLL (https://orcid.org/0000-0001-7669-7236)

CS (https://orcid.org/0000-0002-4120-4662)

PD (https://orcid.org/0000-0003-3700-485X)

AT (https://orcid.org/0000-0001-6690-748X)

Abbreviation title: Preliminary ERT surveys of mock-up EBS

Abstract:

Geophysical Electrical Resistivity Tomography (ERT) is a promising measurement technique for non-intrusive monitoring of Engineered Barrier System (EBS) during the operational phase of geological disposal of high-level radioactive waste. Electrical resistivity is sensitive to water content and temperature, which are the key variables characterising the response of the EBS. In order to assess the technology readiness level of the ERT technique for EBS operational monitoring, a field demonstrator has been developed at the URL in Tournemire (France) within the project 'Modern 2020'. Preliminary ERT surveys were carried out in January and November 2017 to establish the background resistivity of the experimental area and assess the quality of electrode installation and survey protocols. Results of the surveys confirmed that the resistivity of the host rock in the demonstrator area is quite homogenous and lower than 100Ωm in accordance with independent measurements carried out in previous campaigns. In addition, the lesson learned from the blank tests allowed identifying key requirements for effective ERT measurements. These include the need for a 3D electrode configuration, bespoke measurement protocols designed on the basis of sensitivity analysis of geometric factors, and collection of reciprocal data for enhanced data quality control.

Key words: Electrical Resistivity Tomography, Engineered Barrier System, monitoring, non-intrusive, geological disposal.

Introduction

Deep geological repository is favoured by many countries as a technically feasible and safe programme for long-term disposal of high-level radioactive waste (Bredehoeft *et al.* 1978). Although the selected host rock varies from country to country, all programmes consider the implementation of an Engineered Barrier Systems (EBS) to directly protect and isolate the waste. The material selected for the buffer surrounding waste canister as well as the material that will be used to seal off the disposal galleries from the shafts leading to the surface is generally based on compacted bentonite or bentonite/sand mixtures (Sellin & Leupin 2014).

The EBS is subjected to an inward water flow from the host rock and an outward heat flux from the radioactive waste (Lin *et al.* 1995; Rothfuchs *et al.* 2004; Jockwer *et al.* 2006; White *et al.* 2017). Monitoring changes in water content and temperature is therefore the key to assess the performance of the EBS. EBS monitoring during the operational period cannot be achieved via wired sensors installed in the buffer because wires can provide a preferential pathway for radionuclide leakage as well as for water (White *et al.* 2017).

Geophysical electrical monitoring is potentially an ideal technique for geophysical diffuse monitoring of the EBS because (i) it can be designed in a non-intrusive fashion,(ii) it allows capturing local anomalies that local sensors cannot spot, and (iii) electrical resistivity is very sensitive to changes in water content and temperature and is therefore very convenient to monitor the EBS (Danielsen & Dahlin 2010; Korteland & Heimovaara 2015; Merritt *et al.* 2016; Carey *et al.* 2017; López-Sánchez *et al.* 2017; Wang *et al.* 2017; Cosenza *et al.* 2007; Hermans *et al.* 2015; Merritt *et al.* 2016; Carey *et al.* 2017; López-Sánchez *et al.* 2017; Wang *et al.* 2017).

Electrical resistivity tomography (ERT) is a well-established geophysical technique that uses injection of electrical currents and measurements of the resulting voltage differential at the earth's surface or in boreholes. This generates pseudo-sections displaying apparent resistivity as a function of the location and electrode spacing, which in turn provides an initial picture of the resistivity distribution. An inversion process of the measured data is necessary for the final interpretation of the resistance data. This process transforms the apparent resistivity into 2D or 3D images of the bulk electrical resistivity of the subsurface model, which is discretised into a distinct number of elements of homogeneous resistivity.

ERT surveys have been routinely used in water exploration and contaminant flow detection (de Lima *et al.* 1995; D. J. LaBrecque *et al.* 1996; Benson *et al.* 1997; Martinez-Pagan *et al.* 2009; Deceuster *et al.* 2013; Ntarlagiannis *et al.* 2016), engineering site investigations (Rucker *et al.* 2009; Sentenac & Zielinski 2009; Banham & Pringle 2011; Jones *et al.* 2012, 2014), location of buried artefacts or structures in archaeological surveys (Tonkov & Loke 2006; Ullrich *et al.* 2007; Negri *et al.* 2008; Leucci & Greco 2012), as well as providing geological and hydrogeological site information (Ganerød *et al.* 2006; Ramachandran *et al.* 2012; Aning *et al.* 2013).

ERT in boreholes has proven useful for environmental investigations (Daily & Owen 1991; Daily *et al.* 1995; D. LaBrecque *et al.* 1996; French *et al.* 2002; Guérin 2005; Deceuster *et al.* 2006; Wilkinson *et al.* 2010). The method has also been demonstrated to be economically efficient when using wells drilled for geotechnical pre-investigation tunnelling sites to obtain information about the geology between the wells (Denis *et al.* 2002). More recently, investigations using ERT in borehole have been extended to a variety of other applications such as the characterization and monitoring of water infiltration (Oberdörster *et al.* 2010; Coscia *et al.* 2011; Hermans *et al.* 2015) and monitoring CO_2 migration (Yang *et al.* 2015; Schmidt-Hattenberger *et al.* 2016).

Previous researches conducted in repository-like conditions have demonstrated the potential of ERT in monitoring the EBS. Rothfuchs *et al.* (2004) could detect the water intake in an experiment conducted in an area at the Aespoe Hard Rock Laboratory (HRL) in Sweden. ERT electrode arrays were installed in the backfill, buffer and rock and the water saturation changes in those three structures were monitored for a few years. Similarly, Furche & Scuster (2014) have used ERT electrodes arrays installed in the Engineered Barrier Emplacement Experiment in Opalinus Clay at the Mont Terri underground laboratory in Switzerland. Several ERT surveys were conducted over the 11 years of operation of the experiment to monitor water intakes in different areas of the experiment. However, in both these experiments, the ERT electrodes were buried inside the EBS and this arrangement is not suitable for operational monitoring of the EBS. To the best of the authors' knowledge, there has been no attempt to date to investigate the use of the ERT technique in a non-intrusive fashion, i.e. with the electrodes positioned outside the EBS.

This paper presents a mock-up scale test (ERT demonstrator) conceived within the EU project 'Modern2020' and implemented at the Underground Research Laboratory (URL) in Tournemire (France). It is intended to assess the capabilities of the Electrical Resistivity Tomography as a non-intrusive technique of monitoring the Engineered Barrier System under conditions as close as possible to the ones expected in the real repository. ERT electrodes were installed in two boreholes drilled at either side of the buffer to perform cross-borehole surveys. In the paper, three preliminary ERT surveys were carried out in January and November 2017 on the shaft before the emplacement of the bentonite. These surveys were aimed at a first assessment of the electrode installation technique, ERT measurement protocols, and inversion procedures.

Description of Tournemire Underground Research Laboratory

Geological context

The French Institute of Radioprotection and Nuclear Safety (IRSN) uses Tournemire URL test site to conduct research on geological disposal of nuclear waste in clay formations (Cabrera *et al.* 2001; Gélis *et al.* 2010; Okay *et al.* 2013). Tournemire URL is located in southern France, in the western border of the Causses Basin (Cabrera *et al.* 2001; Okay *et al.* 2013).

Fig. 1 shows the geological cross section of Tournemire. According to Okay et al. (2013) the intermediate formation, where the tunnel is located, correspond to marls and clay-rocks and is a good analogue of the Callovo-Oxfordian clay-rock in the Paris Basin, which is considered to be a potential host for the long-term storage of nuclear wastes in France.

An old railway tunnel and six galleries are used to study the Toarcian formation (**Fig. 2**). In general, the Toarcian formation is mainly composed of illite (5–15% weight fraction), illite/smectite mixed-layer minerals (5–10% with a relative proportion of smectite of about 10%), chlorite (1–5%) and kaolinite (15–20%). This formation also contains 10–20% of quartz grains (weight fraction), 10–40% of carbonates (mainly composed of calcite with traces of dolomite and siderite) and 2–9% (in weight) of pyrite disseminated in the clay matrix spreading until 160 m deep from the tunnel (Cabrera *et al.* 2001; Okay *et al.* 2013).

The North-08 gallery

The area selected for the ERT demonstrator at the experimental site in Tournemire URL was the North-08 Gallery. The horseshoe cross-section of the North gallery is 3.7m tall and 4m wide along the floor. This gallery is 20m long oriented north-south (Fig. 2).

On the left, approximately 3m of the area designated for the ERT demonstrator, there is a water infiltration experiment (WT-1) in progress, and on the right, approximately 5m of the ERT demonstrator there is an empty borehole (GN1) of 0.1m in diameter and 7.15m long, located at 1.4m from the gallery floor.

Overview of the ERT demonstrator stages

The project was divided into three main stages. First stage, namely Stage 0, consisted of performing two blank tests before the installation of the EBS to establish the background resistivity of the rock mass. Blank test 1 comprised 2D surface measurements from the North-08 Gallery wall prior to the drilling of left and right boreholes and blank test 2 constituted borehole measurements carried out from the left and right boreholes. Then, in Stage 1, a shaft for the installation of the EBS was drilled and blank test 3 was carried out (**Fig. 3**).

The shaft is 60cm in diameter and approximately 9.05m long. The EBS is constituted by a 4m long mixture of bentonite pellets and powder, namely mixture 3, provided by NAGRA (Garitte *et al.* 2015). The average dry density of the pouring material is 1.45g/cm^3 (Garitte *et al.* 2015). Fig. 4 shows the particle size distribution of the material. The EBS will be closed off with a 2m long concrete plug. Hydration mats will be placed on both ends of the EBS and a heater on the bottom end. Two small access boreholes (**Fig. 2**) will be drilled perpendicular to the longitudinal direction of the buffer to allow the installation of 16 local sensors: 8 Time Domain Reflectometry (TDR) and 8 temperature sensors, to measure water content and temperature as a way of cross-checking the geophysical measurements. For research purposes two lines of

16 electrodes each (0.24m spacing) will be buried inside the main shaft as well. The cross section of the EBS designed for this mock-up test and the instruments setup can be seen in Fig. 5. The installation of the EBS is scheduled to take place in July 2018**Error! Reference source not found.**.

The last stage, Stage 2, consists of regularly monitoring the changes in water content and temperature induced in the EBS using the local sensors and ERT measurements.

Several challenges surround this research experiment amongst them are: (1) electrodes contact resistance problems (Day-Lewis *et al.* 2008; Danielsen & Dahlin 2010; Deceuster *et al.* 2013). The electrodes are installed in boreholes drilled in the rock. Usually, water is added within the borehole to ensure contact in these surveys. However, this resource is not an option for the ERT demonstrator since the electrode boreholes in question are horizontal. It is not possible to keep water in horizontal boreholes, thus continuous injection of water would be necessary in this situation, which would perturb the experiment; (2) data collection and processing (Oldenborger *et al.* 2005; Day-Lewis *et al.* 2008; Wilkinson *et al.* 2008; Deceuster *et al.* 2013). Borehole surveys involve several uncertainties, such as: position and alignment of electrodes, selection of the most appropriate arrays and measurements repeatability; (3) resolution and sensitivity of ERT in boreholes (D. LaBrecque *et al.* 1996; Danielsen & Dahlin 2010; Tso *et al.* 2017).

Data collection of preliminary surveys

The main characteristics of the 2D ERT survey carried out during blank test 1 are presented in Table 1. ARES II unit, manufactured by GF Instruments, was used for the data collection of this blank test.

Two boreholes of 10cm in diameter and approximately 9.0m in length were drilled 1.20m apart, on either side of the position of the EBS, accommodating 32 electrodes spaced at 0.29m, within an inflatable PVC tube (Fig. 6), designed and manufactured by IRSN team. The inflatable system ensures contact between the electrodes and the borehole wall, as the injection of water into the boreholes would potentially disturb the resistivity of the study area hence it is out of question for this experiment. Cross-borehole measurements had been planned for blank test 2, however one of the connectors manufactured to enable the communication between the electrodes and ARES II unit did not work. As an alternative in-line borehole surveys (Fig. 7a) were performed in each borehole individually and the data collected from both boreholes was combined. The multiplexer that accompanies this unit allows the connection of 48 electrodes in total (2 x 24 electrodes), hence the 8 most superficial electrodes in each borehole were not used in these measurements (Fig. 7a). Cross-borehole measurements were also performed using TERRAMETER LS ABEM unit including all 64 electrodes. For lack of familiarity with TERRAMETER LS ABEM unit at the time of blank test 2, the array used was a combination of AM-BN (Fig. 7b) - where A and B are current electrodes and M and N are potential electrodes - and AB-MN (Fig. 7c), that had been developed and implemented into the unit specifically for a previous IRSN research project.

Although part of the data collection of blank test 2 has been made on the boreholes independently using in-line borehole arrays, the data collected using ARES II and TERRAMETER LS ABEM units have been processed together in cross-borehole format (values of geometric factor and hence resistivity were recalculated).

Prior to blank test 3, the shaft was drilled and two new sets of 32 electrodes each were designed, manufactured and installed into the boreholes by IRSN team**Error! Reference source not found.**. Cross borehole measurements were carried out using TERRAMETER LS ABEM unit. The array used was AM-BN (Fig. 7b), based on experience gained from blank test 2 and recommendations of other researches (Day-Lewis *et al.* 2008; Wilkinson *et al.* 2008).

Results and discussions

Data quality

Contact resistance checks were carried out prior to the data collection of each survey. For the 2D surface survey, a paste of bentonite was used to coat the electrodes wherever needed to improve contact resistance. However, this resource could not be used for borehole surveys. As suggested by Day-Lewis *et al.* (2008), cut-offs of 50kΩ for borehole data and 20kΩ for surface data were considered, since higher values may indicate that only a limited current can be injected for that electrode pair. The largest contact resistance recorded for blank test 1 was 3.5 kΩ, i.e. all electrodes were included. The contact resistance collected before blank tests 2 and 3 are plotted in Fig. 8. Some electrodes showed contact resistance larger than 50 kΩ and were discarded.

Both units used in the three blank tests offer stacking procedure. The stack procedure consists of collecting each quadripole several times and averaging the results. This procedure has two clear advantages: (1) random noise is averaged out, which improves signal-to-noise ratio and (2) the standard deviation (stacking error) provides means of quantifying error and defining data weights for inversion. For all blank tests carried out, the minimum number of stacking selected was 4 and the maximum was 8. The maximum variation coefficient accepted was 2%. In practical terms, this means that if the average standard deviation of the first 4 measurements for a quadripole is greater than 2% then more measurements are going to be collected for that quadripole up until the maximum number selected (equal to 8 in this case). The standard deviation of all data collected is then calculated and recorded, regardless of whether the value is higher or lower than 2%. Data with stacking errors larger than 3% were eliminated (Day-Lewis *et al.* 2008).

The mean stacking error of blank test 1 was 0.16% and no recorded data had stacking errors larger than 3%. Fig. 9 illustrates the stacking error distribution of blank test 2 and blank test 3. The mean stacking error and the percentage of data larger than 3% obtained for each test carried out are detailed in Table 2. The lower stacking errors observed in blank test 1 compared to the blank tests 2 and 3 can be justified by two main reasons, (i) the approaches used to improve the electrode contacts and (ii) the survey type. In blank test 1, where surface surveys were carried out, bentonite was used to improve the contact between the electrode and the rock, while the electrode contacts of the other two blank tests, 2 and 3, were ensured only by pressure. In addition, the protocols used for blank test 1 were well-established 2D surface protocols with attested good sensitivities while the protocols of blank tests 2 and 3 had not been yet properly adapted.

The length of the current pulse was selected equal to 300ms. Reciprocal measurements, which involve swapping current and voltage electrode pairs, could not be collected due to time constrains during the surveys.

Another concern for borehole surveys is the geometric factors, K. Geometric factors are numerical multipliers used to convert the resistance *R* (voltage to current ratio) in apparent resistivity ρ_a:

$$\rho_a = K.R$$

The geometric factor depends on the geometry of each electrode spacing setup. For borehole surveys Wilkinson *et al.* (2008) demonstrated that large geometric sensitivities of an electrode configuration occur when the geometric factor, K, changes rapidly with position. In turn, this occurs when K is close to singular. In addition, K will also be large in the vicinities of the singularity. Due to several operational issues, the arrays used for data collection during blank test 2 were not the most suitable. Hence, a considerable amount of data collected presented large K values, therefore the data collected in blank test 2 were filtered based on the geometric factor, i.e. data associated with geometric factors larger than $250m^{-1}$ were discarded. Fig. 10 shows the distribution of apparent resistivity before and after filtering out measurements with high geometric factors for blank tests 2.

Overall, contact resistance, stacking errors, and geometric factor errors were the three features used to filter the data collected in the surveys performed for the ERT demonstrator. The percentage of total data removed from each survey is shown in Table 2.

Inversions

To investigate the benefits of filtering data according to the strategies discussed in the previous section, inversions were performed on both the original and filtered data sets for comparison. Table 2 shows the Root Mean Square (RMS) errors obtained from these inversions.

Inversions were performed using the commercially available software package Res2DInv® (Loke 2015). After carefully testing numerous inversion settings (Day-Lewis *et al.* 2008), the default settings proved to be the most appropriate one. These settings were used for all control parameters, which were kept identical for each inversion.

Tomograms plots generated from filtered data sets of blank test 1 – 2D surface survey Schlumberger array; blank tests 2 – in- and cross-hole array; and blank test 3 – cross-hole array are shown in Fig. 11, Fig. 12 and Fig. 13 respectively. The geometric location of WT-1 and GN1 are highlighted in the tomogram of blank test 1 (Fig. 11) as well as the future position of the main shaft and electrodes boreholes that at this stage had not yet been drilled.

The result of blank test 1 presented in Fig. 11 shows that higher values of resistivity are found at the surface. This is reasonable since the rock face exposed to the gallery presents lower degree of saturation and, hence, higher values of resistivity. Below and around 0.5m the resistivity of the rock mass is fairly homogeneous with values lower than 100Ωm, which is consistent with the results shown in blank tests 2 (Fig. 12) and 3 (Fig. 13) and also with the resistivity measured in the laboratory on core samples extracted from both boreholes (average of 40Ωm). Cosenza *et al.* (2007) and Gélis *et al.* (2016) also reported similar results in terms of resistivity of Tournemire's core samples and 2D ERT surveys in Tournemire URL respectively.

In blank test 1, there is an area of high resistivity (between chainage 14 and 17m) that could suggest the presence of an anomaly. This anomaly could be related to the WT-1 shaft, which is empty in the first 3.4m. There is another area of high resistivity in the model between chainage 12 and 13.2m that extends to almost 2m into the wall. From all the field data and information gathered so and made available by the IRSN team, there is nothing in this latest segment that could justify such a high resistivity. Thus, a possible interpretation of these results is that the high resistivity along the segment 14 and 17m is an artefact and WT-1 shaft is actually associated with the high resistivity area between 12 and 13.2m. To investigate the issue further, an inversion was tested with a priori resistivity information of WT-1 and GN1. The inversion results have created an even larger artefact of high resistivity over almost the whole model and the RMS error of this inversion has doubled. As the RMS indicates the mismatch between the forward and calculated models, these results were not considered satisfactory. Therefore, it was speculated that the problem stemmed from a 2D inversion algorithms used to invert data of 3D bodies located outside the image plane (Nimmer *et al.* 2008).

The empty shaft of WT-1 presents virtually infinite resistivity and is by-passed by the current, which follows more conductive paths. The stainless steel lid (35cm thick) is located at 3.4m depth into the WT-1 shaft likely affecting the resistivity measurements (although the lid itself is outside of the area of the inversion). Furthermore, WT-1 is located towards the edge of the area covered by the inversion model, which is highly affected by boundary effects. As a result, WT-1 is not clearly detected.

Blank test 2 (Fig. 12) was a combination of data collected from arrays involving in-hole and cross-hole quadripoles combinations. The data was processed in cross-borehole format, treated according to the procedure described in the data quality session and inverted. Fig. 12 shows that the resistivity between the two boreholes is somehow homogeneous and lower than 100Ωm. The area of higher resistivity around the electrodes and in the middle of the model (around 5m depth) is most likely due to artefacts created by the noise survey. A considerable number of negative apparent resistivity data was collected during blank test 2. This negative apparent resistivity does not appear to be real, since virtually no negative apparent resistivity remained after filtering the data according to the data quality procedure (Fig. 10).

Blank test 3 (Fig. 13) has an empty shaft (0.6cm in diameter and 9.05m in length) in the middle of the cross borehole model, which should be characterised by high resistivity values. However, higher resistivity values (greater than 500Ωm) can only be spotted in the first 2.0m of the model, close to the gallery wall. This inconsistency was expected due to the presence of the shaft. The current flow is expected to act three dimensionally avoiding the volume of high resistivity. Inverting the data collected in the blank test 3 using a 3D algorithm would not improve the results. The problem of this survey is the data collection itself. The main shaft represents a 3D body characterised by virtually infinite resistivity. Although there has been a significant improvement in the protocol used for blank test 3 when compared to the one used on blank test 2, the site characteristics were very difficult to capture using 2D surveys.

To test this hypothesis a 3D synthetic model was created reproducing the site characteristics (Fig. 14a). The model has 2.4m x 2.6m x 10m with background resistivity of 40Ωm, replicating the resistivity of the core rock samples tested in laboratory, and a shaft of 0.6m x 0.6m x 9.05m in the middle with resistivity of 1E+15Ωm, representing the empty shaft. The synthetic data were created in 3D, without adding noise, but the protocol used was the same of blank test 3. Firstly, the data were inverted using a 3D algorithm (RES3DInv® - (Loke 2017)), and the tomography result can be observed in Fig. 14b. Apart from a few artefacts of high resistivity around the edges, the resistivity of the whole model is homogeneous and around 100Ωm. Therefore, the high resistivity body representing the main shaft is not characterised in the tomography results. Then, the same data were inverted using a 2D algorithm and the tomography result is presented in Fig. 14c. The highest resistivity value observed is 250Ωm in the centre towards the bottom of the model. Outside this area, the resistivity of the model is homogenous and around 100Ωm. The higher resistivity observed in the 2D inverted model is not enough to characterise precisely the empty shaft. Therefore, the outcome shows that the 2D protocol used in blank test 3 was unable to capture the main empty shaft regardless of the inverted algorithm used.

For the monitoring stages of this experiment, protocols need to be improved and tested by means of forward modelling and sensitivity analysis to ensure the quality of the data collected and consistency of the inversion results. The possibility of adding a third borehole to install electrodes at the top of the main shaft is currently being examined. This additional set of electrodes could improve the tomography images. In this way, the data can be collected in a real 3D fashion and inverted using 3D algorithm.

Conclusions

This paper has presented the preliminary Electrical Resistivity Tomography surveys of the ERT demonstrator carried out in Tournemire URL. This demonstrator is aimed to investigate the potential of ERT as non-invasive monitoring of the thermo-hydraulic response of the Engineered Barrier System (EBS) during the operational stage. The blank test surveys have allowed characterising the resistivity of the host rock and, most importantly, have allowed identifying the most suitable ERT protocols to be adopted in the next stages of the project when the EBS will be put in place.

Results obtained from laboratory experiments performed on core samples extracted from different depths during the drilling process suggested that the resistivity of the host rock is homogeneous and around 40Ωm. The homogeneously of the host rock was indeed confirmed by blank test 1 and blank test 2, with consistent resistivity values lower than 100Ωm. The methodology developed for the electrode installation based on the use of PVC half-tubes pushed against the borehole wall by inflatable pipes has proved to be successful. However, electrodes contact resistance remains a challenge that need to be addressed.

Inspection of the tomograms derived from in- and cross-hole array has highlighted the drawbacks of the protocols used and suggested the modifications to be introduced in the next stage of the experimental programme. In particular, the lesson learned from the blank tests allowed the following actions to be put in place:

- Since the problem is clearly 3D, electrodes should be placed in 3D configuration, i.e. a third electrode array should be added at the top of the main shaft to complement the two arrays located laterally to the main shaft (on the left-hand and right-hand sides respectively). In this way, data can be collected in 3D fashion and inverted using 3D inversion algorithms. This measure should reduce the appearance of artefacts and allow generating enhanced tomography images;
- New measurement protocols suitable for in-hole and cross-hole need to be developed to allow for more efficient data collection in terms of measurement time and adequate geometric factors. To ensure the quality of the measurement protocols, sensitivity analysis should be carried out on various protocol datasets complemented by similar analysis using synthetic data via forward model;
- Reciprocal data should be collected to allow for enhanced data quality control.

Acknowledgements

The authors wish to acknowledge the support of the European Commission via the project MODERN2020 'Development and Demonstration of monitoring strategies and technologies for geological disposal’ (Grant Agreement number: 662177-Modern2020-NFRP-2014-2015) under the H2020 Euratom Research and Training Programme. We also thank ANDRA and IRSN for the funding support. And we thank Patrice Desveaux and Bruno Combes for their support in the experiments and for manufacturing the electrodes.

References

Aning, A.A., Tucholka, P. & Danuor, S.K. 2013. 2D Electrical Resistivity Tomography (ERT) Survey using the Multi-Electrode Gradient Array at the Bosumtwi Impact Crater ,. **3**, 12–27.

Banham, S. & Pringle, J.K. 2011. Geophysical and intrusive site investigations to detect an abandoned coal-mine access shaft, Apedale, Staffordshire, UK. *Near Surface Geophysics*, **9**, 483–496.

Benson, A.K., Payne, K.L. & Stubben, M.A. 1997. Mapping groundwater contamination using dc resistivity and VLF geophysical methods–A case study. *Geophysics*, **62**, 80–86, https://doi.org/10.1190/1.1444148.

Bredehoeft, J.D., England, A.W., Stewart, D.B., Trask, N.J. & Winograd, I.J. 1978. *Geologic Disposal of High-Level Radioactive Wastes- Earth-Science Perspectives*.

Cabrera, J., Beaucaire, C., et al. 2001. *Projet Tournemire – Synthèse Des Programmes de Recherche 1995–1999. Report #IPSN DPRE/SERGD*. Paris.

Carey, A.M., Paige, G.B., Carr, B.J. & Dogan, M. 2017. Forward modeling to investigate inversion artifacts resulting from time-lapse electrical resistivity tomography during rainfall simulations. *Journal of Applied Geophysics*, **145**, 39–49, https://doi.org/10.1016/j.jappgeo.2017.08.002.

Coscia, I., Greenhalgh, S.A., et al. 2011. 3D crosshole ERT for aquifer characterization and monitoring of infiltrating river water. *Geophysics*, **76**, G49–G59, https://doi.org/10.1190/1.3553003.

Cosenza, P., Ghorbani, A., Florsch, N. & Revil, A. 2007. Effects of drying on the low-frequency electrical properties of Tournemire argillites. *Pure and Applied Geophysics*, **164**, 2043–2066, https://doi.org/10.1007/s00024-007-0253-0.

Daily, W. & Owen, E. 1991. Cross-borehole resistivity tomography. *Geophysics*, **56**, 1228–1235.

Daily, W., Ramirez, A., LaBrecque, D. & Barber, W. 1995. Electrical resistance tomography experiments at the Oregon Graduate Institute. *Journal of Applied Geophysics*, **33**, 227–237, https://doi.org/10.1016/0926-9851(95)90043-8.

Danielsen, B.E. & Dahlin, T. 2010. Numerical modelling of resolution and sensitivity of ERT in horizontal boreholes. *Journal of Applied Geophysics*, **70**, 245–254, https://doi.org/10.1016/j.jappgeo.2010.01.005.

Day-Lewis, F.D., Johnson, C.D., Singha, K. & Lane Jr, J.W. 2008. *Best Practices in Electrical Resistivity Imaging: Data Collection and Processing, and Application to Data from Corinna, Maine*.

de Lima, O.A.L., Sato, H.K. & Porsani, M.J. 1995. Imaging industrial contaminant plumes with resistivity techniques. *Journal of Applied Geophysics*, **34**, 93–108, https://doi.org/10.1016/0926-9851(95)00014-3.

Deceuster, J., Delgranche, J. & Kaufmann, O. 2006. 2D cross-borehole resistivity tomographies below foundations as a tool to design proper remedial actions in covered karst. *Journal of Applied Geophysics*, **60**, 68–86, https://doi.org/10.1016/j.jappgeo.2005.12.005.

Deceuster, J., Kaufmann, O. & Camp, M. Van. 2013. Automated identification of changes in electrode contact properties for long-term permanent ERT monitoring experiments. *Geophysics*, **78**, E79–E94, https://doi.org/10.1190/GEO2012-0088.1.

Denis, A., Marache, A., Obellianne, T. & Breysse, D. 2002. Electrical resistivity borehole measurements: Application to an urban tunnel site. *Journal of Applied Geophysics*, **50**, 319–331, https://doi.org/10.1016/S0926-9851(02)00150-7.

French, H.K., Hardbattle, C., Binley, A., Winship, P. & Jakobsen, L. 2002. Monitoring snowmelt induced unsaturated flow and transport using electrical resistivity tomography. *Journal of Hydrology*, **267**, 273–284, https://doi.org/10.1016/s0022-1694(02)00156-7.

Furche, M. & Scuster, K. 2014. *Long-Term Performance of Engineered Barrier Systems PEBS*.

Ganerød, G.V., Rønning, J.S., Dalsegg, E., Elvebakk, H., Holmøy, K., Nilsen, B. & Braathen, A. 2006. Comparison of geophysical methods for sub-surface mapping of faults and fracture zones in a section of the Viggja road tunnel, Norway. *Bulletin of Engineering Geology and the Environment*, **65**, 231–243, https://doi.org/10.1007/s10064-006-0041-6.

Garitte, B., Weber, H. & Müller, H.R. 2015. *Requirements, Manufacturing and QC of the Buffer Components Report LUCOEX – WP2*.

Gélis, C., Revil, A., et al. 2010. Potential of electrical resistivity tomography to detect fault zones in limestone and argillaceous formations in the experimental platform of Tournemire, France. *Pure and Applied Geophysics*, **167**, 1405–1418, https://doi.org/10.1007/s00024-010-0097-x.

Gélis, C., Noble, M., Cabrera, J., Penz, S., Chauris, H. & Cushing, E.M. 2016. Ability of High-Resolution Resistivity Tomography to Detect Fault and Fracture Zones: Application to the Tournemire Experimental Platform, France. *Pure and Applied Geophysics*, **173**, 573–589, https://doi.org/10.1007/s00024-015-1110-1.

Guérin, R. 2005. Borehole and surface-based hydrogeophysics. *Hydrogeology Journal*, **13**, 251–254, https://doi.org/10.1007/s10040-004-0415-4.

Hermans, T., Wildemeersch, S., Jamin, P., Orban, P., Brouyère, S., Dassargues, A. & Nguyen, F. 2015. Quantitative temperature monitoring of a heat tracing experiment using cross-borehole ERT. *Geothermics*, **53**, 14–26, https://doi.org/10.1016/j.geothermics.2014.03.013.

Jockwer, N., Wieczorek, K., Miehe, R. & Diaz, A.M.F. 2006. *Heater Test in the Opalinus Clay of the Mont Terri URL Gas Release and Water Redistribution*.

Jones, G., Zielinski, M. & Sentenac, P. 2012. Mapping desiccation fissures using 3-D electrical resistivity tomography. *Journal of Applied Geophysics*, **84**, 39–51, https://doi.org/10.1016/j.jappgeo.2012.06.002.

Jones, G., Sentenac, P. & Zielinski, M. 2014. Desiccation cracking detection using 2-D and 3-D Electrical Resistivity Tomography : Validation on a fl ood embankment. *Journal of Applied Geophysics*, **106**, 196–211, https://doi.org/10.1016/j.jappgeo.2014.04.018.

Korteland, S.A. & Heimovaara, T. 2015. Quantitative inverse modelling of a cylindrical object in the laboratory using ERT: An error analysis. *Journal of Applied Geophysics*, **114**, 101–115, https://doi.org/10.1016/j.jappgeo.2014.10.026.

LaBrecque, D., Miletto, M., Daily, W., Ramirez, A. & Owen, E. 1996. The effects of noise on Occam's inversion of resistivity tomography data. *Geophysics*, **61**, 538–548.

LaBrecque, D.J., Ramirez, A.L., Daily, W.D., Binley, A.M. & Schima, S.A. 1996. ERT monitoring of environmental remediation processes. *Measurement Science and Technology*, **7**, 375–383, https://doi.org/10.1088/0957-0233/7/3/019.

Leucci, G. & Greco, F. 2012. 3D ERT Survey to Reconstruct Archaeological Features in the Subsoil of the ‘ Spirito Santo ’ Church Ruins at the Site of Occhiolà (Sicily , Italy). *Archaeology*, **1**, 1–6, https://doi.org/10.5923/j.archaeology.20120101.01.

Lin, W., Wilder, D.G., et al. 1995. A Heated Large Block Test for High Level Nuclear Waste Management 2. *In*: *2nd International Conference on Mechanics of Jointed and Faulted Rock (MJFR-2)*. Vienna.

Loke, M.H. 2015. RES2DINV. Rapid 2-D Resistivity & IP inversion using the least-squares method. 127P.

Loke, M.H. 2017. *Rapid 3-D Resistivity & IP Inversion Using the Least-Squares Method*.

López-Sánchez, M., Mansilla-Plaza, L. & Sánchez-de-laOrden, M. 2017. Geometric factor and influence of sensors in the establishment of a resistivity-moisture relation in soil samples. *Journal of Applied Geophysics*, **145**, 1–11, https://doi.org/10.1016/j.jappgeo.2017.07.011.

Martinez-Pagan, P., Faz, A. & Aracil, E. 2009. The use of 2D electrical tomography to assess pollution in slurry ponds of the Murcia region, SE Spain. *Near Surface Geophysics*, **7**, 49–61, https://doi.org/10.3997/1873-0604.2008033.

Merritt, A.J., Chambers, J.E., Wilkinson, P.B., West, L.J., Murphy, W., Gunn, D. & Uhlemann, S. 2016. Measurement and modelling of moisture-electrical resistivity relationship of fine-grained unsaturated soils and electrical anisotropy. *Journal of Applied Geophysics*, **124**, 155–165, https://doi.org/10.1016/j.jappgeo.2015.11.005.

Negri, S., Leucci, G. & Mazzone, F. 2008. High resolution 3D ERT to help GPR data interpretation for researching archaeological items in a geologically complex subsurface. *Journal of Applied Geophysics*, **65**, 111–120, https://doi.org/10.1016/j.jappgeo.2008.06.004.

Nimmer, R.E., Osiensky, J.L., Binley, A.M. & Williams, B.C. 2008. Three-dimensional effects causing artifacts in two-dimensional, cross-borehole, electrical imaging. *Journal of Hydrology*, **359**, 59–70, https://doi.org/10.1016/j.jhydrol.2008.06.022.

Ntarlagiannis, D., Robinson, J., Soupios, P. & Slater, L. 2016. Field-scale electrical geophysics over an olive oil mill waste deposition site: Evaluating the information content of resistivity versus induced polarization (IP) images for delineating the spatial extent of organic contamination. *Journal of Applied Geophysics*, **135**, 418–426, https://doi.org/10.1016/j.jappgeo.2016.01.017.

Oberdörster, C., Vanderborght, J., Kemna, A. & Vereecken, H. 2010. Investigating Preferential Flow Processes in a Forest Soil Using Time Domain Reflectometry and Electrical Resistivity Tomography. *Vadose Zone Journal*, **9**, 350–361, https://doi.org/10.2136/vzj2009.0073.

Okay, G., Cosenza, P., Ghorbani, A., Camerlynck, C., Cabrera, J., Florsch, N. & Revil, A. 2013. Localization and characterization of cracks in clay-rocks using frequency and time-domain induced polarization. *Geophysical Prospecting*, **61**, 134–152, https://doi.org/10.1111/j.1365-2478.2012.01054.x.

Oldenborger, G.A., Routh, P.S. & Knoll, M.D. 2005. Sensitivity of electrical resistivity tomography data to electrode position errors. *Geophys. J. Int.*, 1–9, https://doi.org/10.1111/j.1365-246X.2005.02714.x.

Ramachandran, K., Tapp, B., Rigsby, T. & Lewallen, E. 2012. Imaging of fault and fracture controls in the arbuckle-simpson aquifer, Southern Oklahoma, USA, through electrical resistivity sounding and tomography methods. *International Journal of Geophysics*, 1–10, https://doi.org/10.1155/2012/184836.

Rothfuchs, T., Miehe, R., Moog, H. & Wieczorek, K. 2004. *Geoelectric Investigation of Bentonite Barrier Saturation*.

Rucker, D.F., Levitt, M.T. & Greenwood, W.J. 2009. Three-dimensional electrical resistivity model of a nuclear waste disposal site. *Journal of Applied Geophysics*, **69**, 150–164, https://doi.org/10.1016/j.jappgeo.2009.09.001.

Schmidt-Hattenberger, C., Bergmann, P., Labitzke, T., Wagner, F. & Rippe, D. 2016. Permanent crosshole electrical resistivity tomography (ERT) as an established method for the long-term CO2monitoring at the Ketzin pilot site. *International Journal of Greenhouse Gas Control*, **52**, 432–448, https://doi.org/10.1016/j.ijggc.2016.07.024.

Sellin, P. & Leupin, O.X. 2014. The use of clay as an engineered barrier in radioactive-waste management - A review. *Clays and Clay Minerals*, **61**, 477–498, https://doi.org/10.1346/CCMN.2013.0610601.

Sentenac, P. & Zielinski, M. 2009. Clay fine fissuring monitoring using miniature geo-electrical resistivity arrays. *Environmental Earth Sciences*, **59**, 205–214, https://doi.org/10.1007/s12665-009-0017-5.

Tonkov, N. & Loke, M.H. 2006. A resistivity survey of a burial mound in the 'Valley of the Thracian Kings'. *Archaeological Prospection*, **13**, 129–136, https://doi.org/10.1002/arp.273.

Tso, C.H.M., Kuras, O., et al. 2017. Improved characterisation and modelling of measurement errors in electrical resistivity tomography (ERT) surveys. *Journal of Applied Geophysics*, **146**, 103–119, https://doi.org/10.1016/j.jappgeo.2017.09.009.

Ullrich, B., Guenther, T. & Ruecker, C. 2007. Electrical Resistivity Tomography Methods for Archaeological Prospection. *Geophysical Prospecting*, 1–7.

Wang, J., Zhang, X. & Du, L. 2017. A laboratory study of the correlation between the thermal conductivity and electrical resistivity of soil. *Journal of Applied Geophysics*, **145**, 12–16, https://doi.org/10.1016/j.jappgeo.2017.07.009.

White, M., Farrow, J. & Crawford, M. 2017. *Deliverable D2.1 : Repository Monitoring Strategies and Screening Methodologies*.

Wilkinson, P.B., Chambers, J.E., Lelliott, M., Wealthall, G.P. & Ogilvy, R.D. 2008. Extreme sensitivity of crosshole electrical resistivity tomography measurements to geometric errors. *Geophysical Journal International*, **173**, 49–62, https://doi.org/10.1111/j.1365-

246X.2008.03725.x.

Wilkinson, P.B., Meldrum, P.I., Kuras, O., Chambers, J.E., Holyoake, S.J. & Ogilvy, R.D. 2010. High-resolution Electrical Resistivity Tomography monitoring of a tracer test in a confined aquifer. *Journal of Applied Geophysics*, **70**, 268–276, https://doi.org/10.1016/j.jappgeo.2009.08.001.

Yang, X., Lassen, R.N., Jensen, K.H. & Looms, M.C. 2015. Monitoring CO2migration in a shallow sand aquifer using 3D crosshole electrical resistivity tomography. *International Journal of Greenhouse Gas Control*, **42**, 534–544, https://doi.org/10.1016/j.ijggc.2015.09.005.

Figure captions

Fig. 1. Geological cross section of Tournemire URL.

Fig. 2. Position of the galleries at the experimental site.

Fig. 3. Overview of ERT demonstrator stages, preliminary surveys – blank tests 1, 2 and 3.

Fig. 4. *Bentonite pellets and powder particle size distribution* (Garitte *et al.* 2015).

Fig. 5. Cross section of *Engineered Barrier System setup.*

Fig. 6. *Scheme of electrodes setup used for blank test 2 and 3 developed by IRSN.*

Fig. 7. (a) ERT protocol used for blank test 2 with ARES II unit – in-line array, (b) ERT protocol used for blank test 2 with TERRAMETER LS – cross-borehole array AM-BN (c) ERT protocol used for blank test 2 with TERRAMETER LS – cross-borehole array AB-MN, where A and B are current electrodes and M and N are potential electrodes.

Fig. 8. *Electrodes resistance contacts (a) blank test 2 and (b) blank test 3.*

Fig. 9. *Stacking errors (a) blank test 2 and (b) blank test 3.*

Fig. 10. *Distribution of apparent resistivity before and after filtering out measurements associated with large geometric factors, black and grey bars respectively, for blank test 2.*

Fig. 11. *Blank test 1: 2D surface survey, Schlumberger array (GN1 and WT-1 indicated by black rectangles and main shaft and electrodes boreholes of ERT demonstrator area indicated by black dashed rectangles).*

Fig. 12. *Blank test 2: borehole survey.*

Fig. 13. *Blank test 3: cross borehole survey (buffer shaft indicated by black rectangle).*

Fig. 14. Synthetic data analysis. (a) 3D model (Model 2.4 x 2.6 x 10m, shaft 0.6 x 0.6 x 9.05m) (b) Perspective and cross section (at same plane where electrode boreholes are) view of 3D Data inverted using 3D algorithm and the AM-BN protocol of Blank test 3 and (c) 3D Data inverted using 2D algorithm and the AM-BN protocol of Blank test 3 (where A and B are current electrodes and M and N potential electrodes).

Table 1. *Main characteristics of blank test 1.*

Electrodes spacing	0.4m
Total number of electrodes	48
Total length	18.8m
Position of electrodes in z-axis	1.4m from the gallery floor
First electrode (El 0) in x-axis	On the right: standing on Gallery North_08 and facing the ERT demonstrator location
Measurement type	2D surface
Unit used	ARES II
Array used	Schlumberger
Electrodes used	Conventional metal sticks (surface)

Table 2. *Summary of number of data collected, stacking errors recorded, percentage of data removed in all blank tests and RMS errors obtained from inversions performed on original and filtered data sets.*

Surveys	Total No. of data	Mean stacking error (%)	Data stacking error > 3% (%)	Data removed (%)	Original data RMS (%)	Filtered data RMS (%)
Blank test 1	522	0.16	0.0	0.0	9.20	-
Blank test 2	1831	6.91	18.51	46.0	30.72	12.69
Blank test 3	1059	2.22	13.4	14.5	7.18	5.64

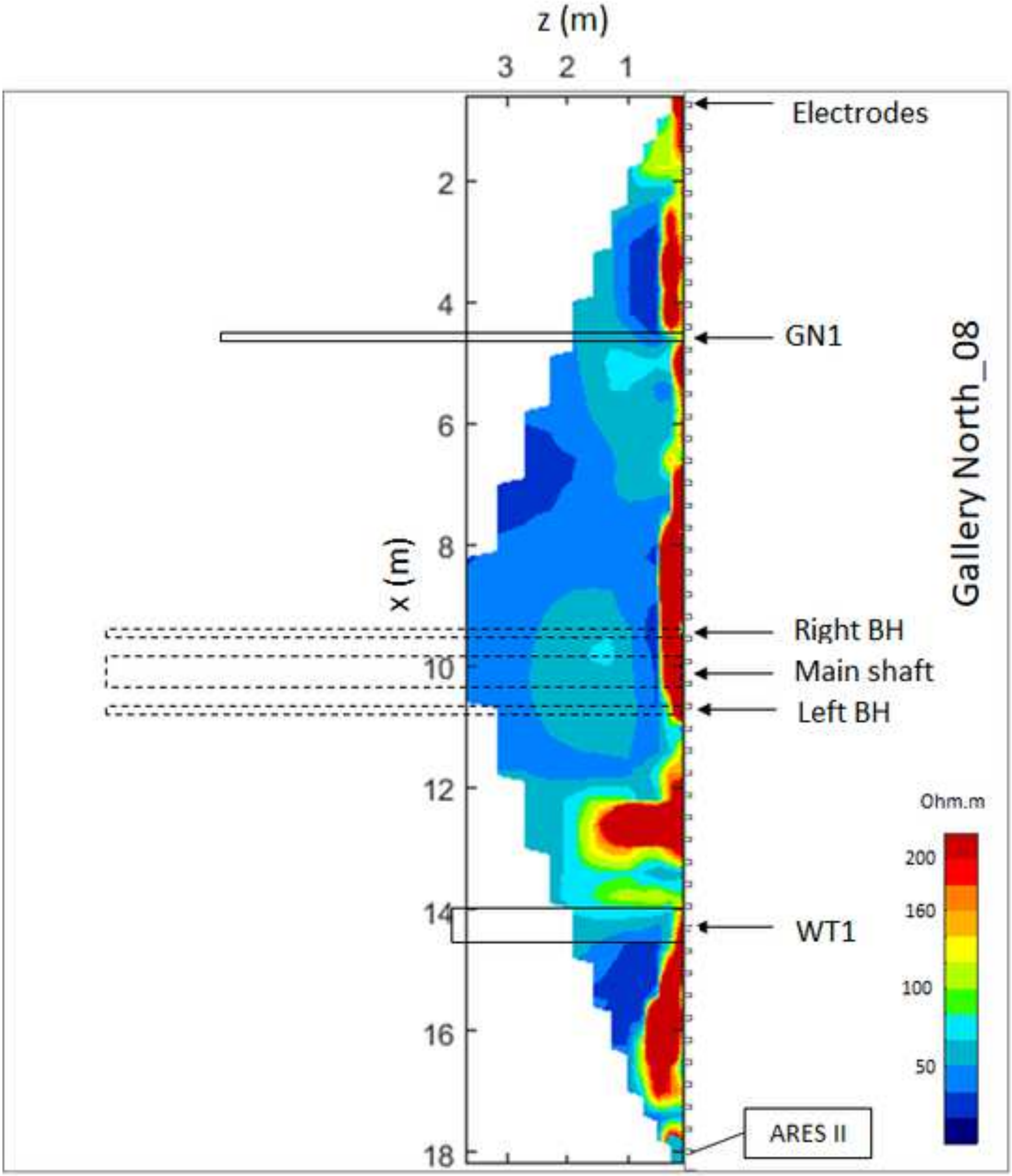
z (m)
3
2
1
Electrodes
2
4
GN1
6
8
x (m)
Gallery North_08
Right BH
10
Main shaft
Left BH
12
Ohm.m
200
160
14
WT1
100
16
50
ARES II
18

Click here to download figure LOPES Figure 12.bmp

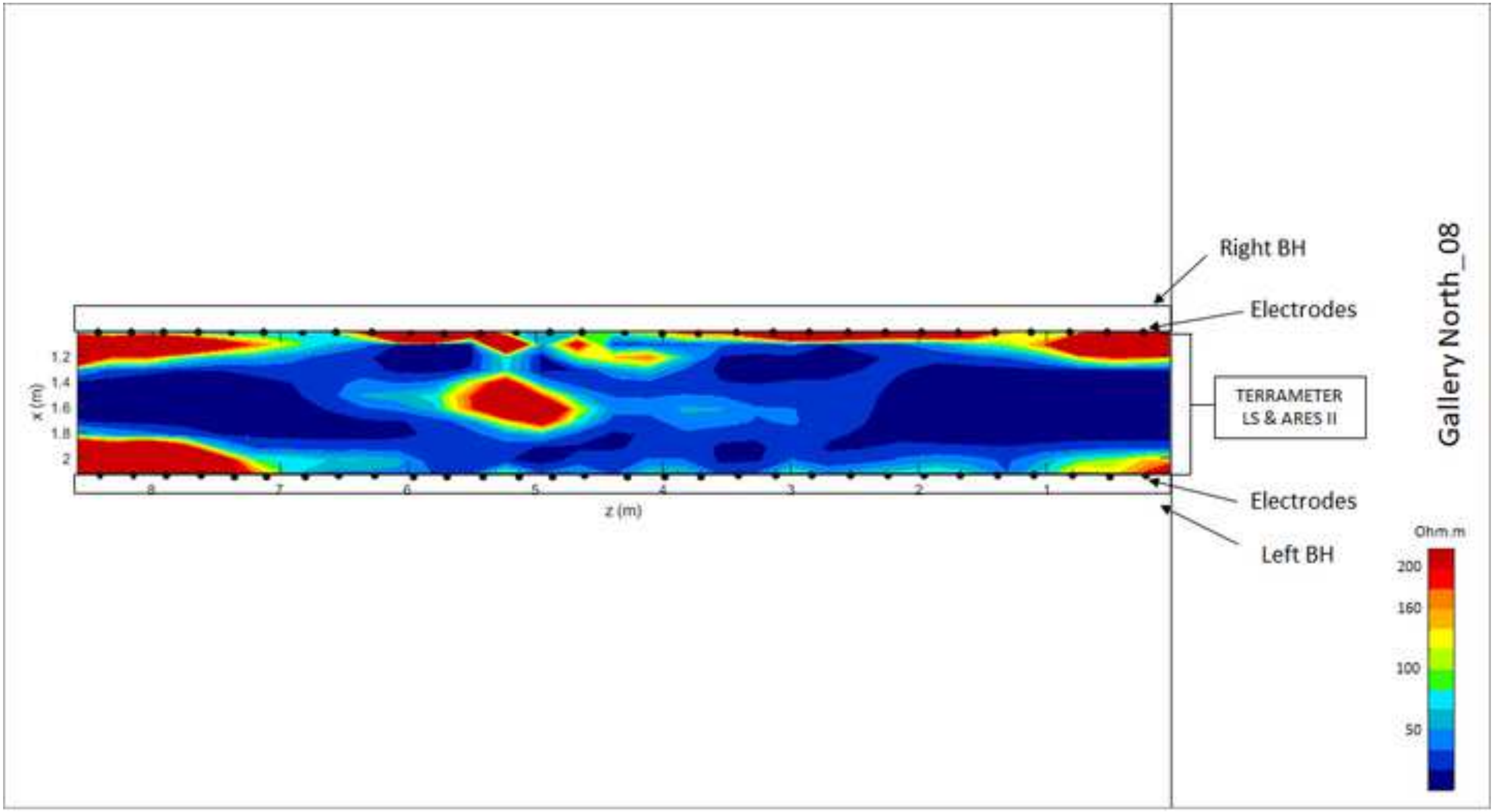

Click here to download figure LOPES Figure 13.bmp

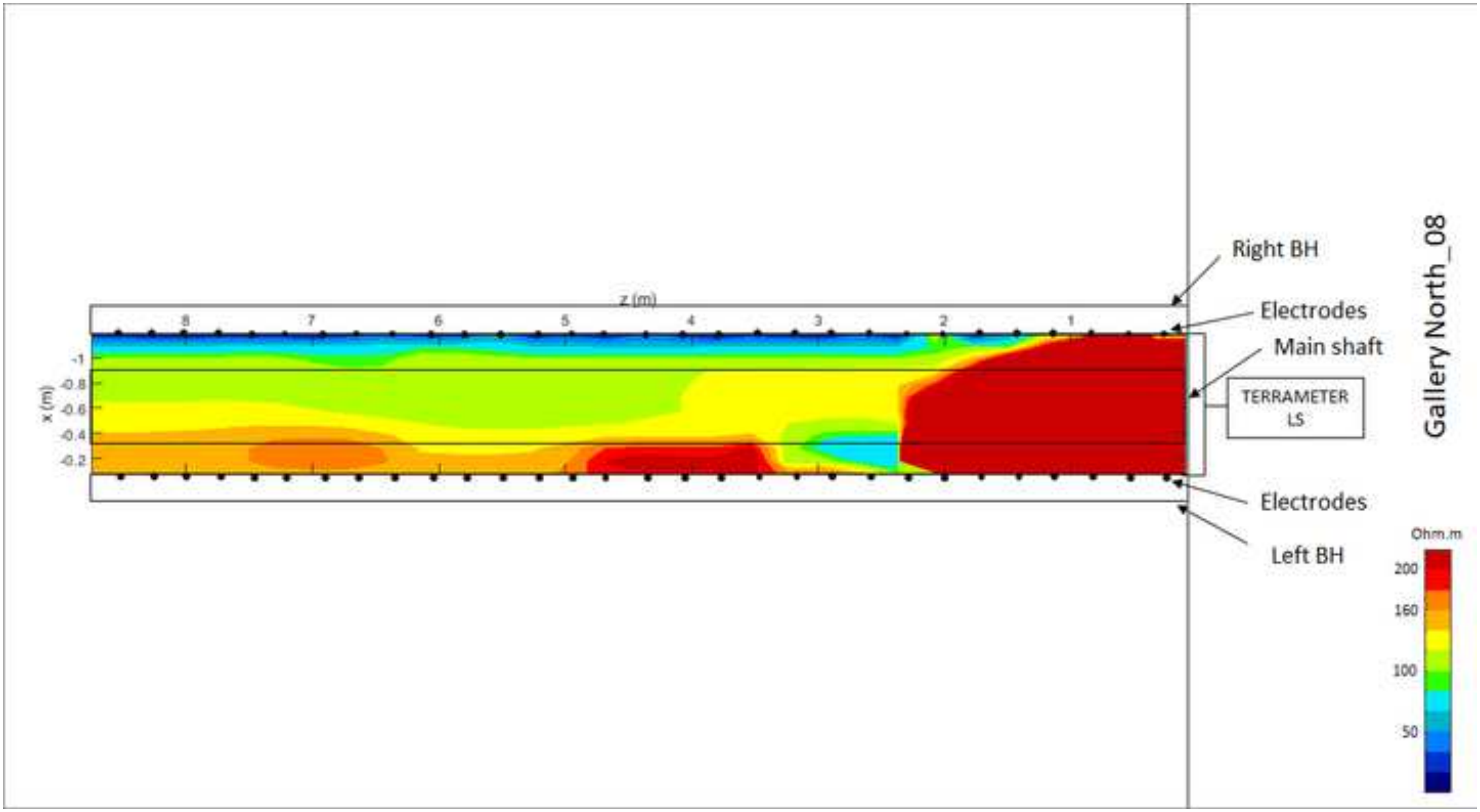

Click here to download figure LOPES Figure 14c.bmp

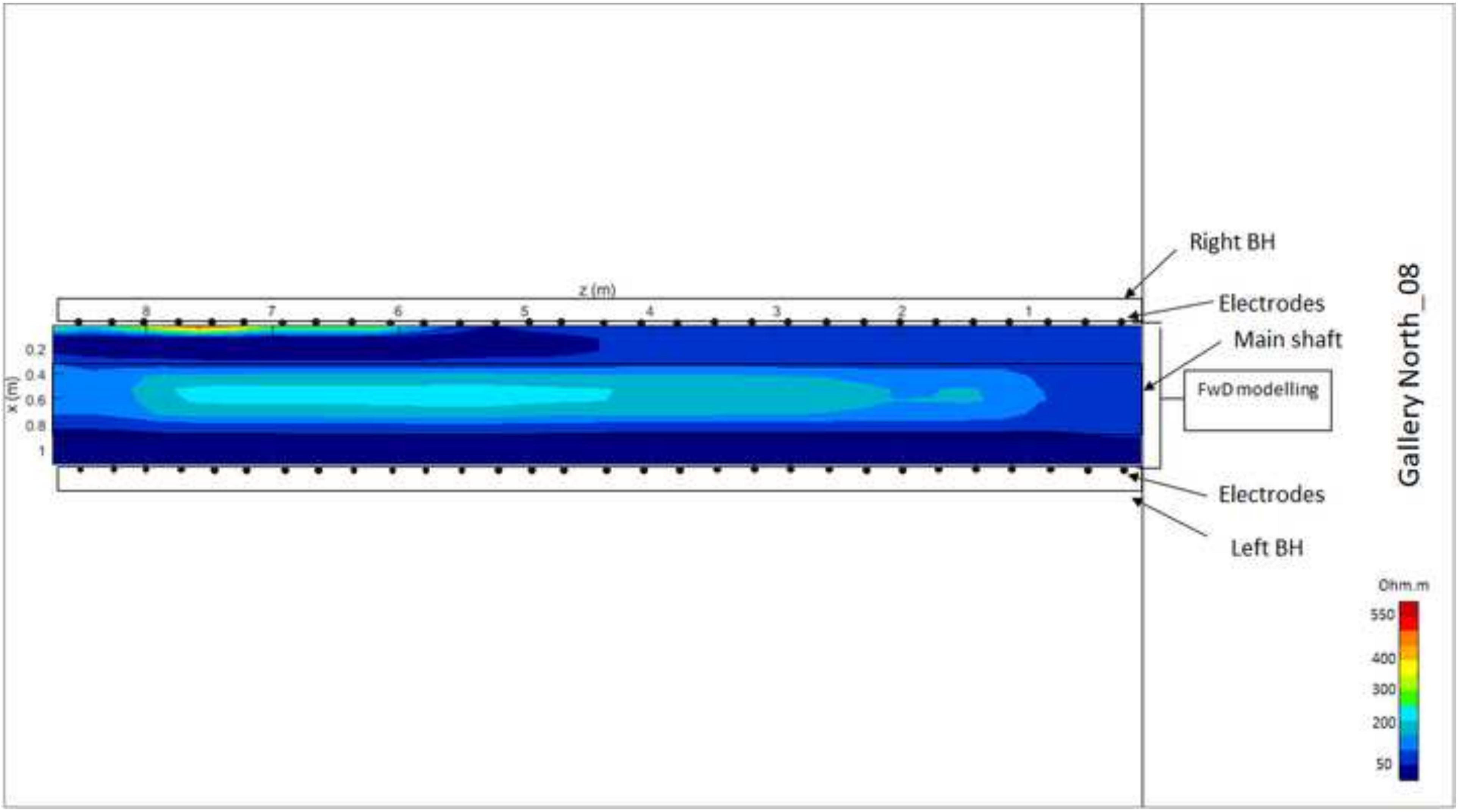

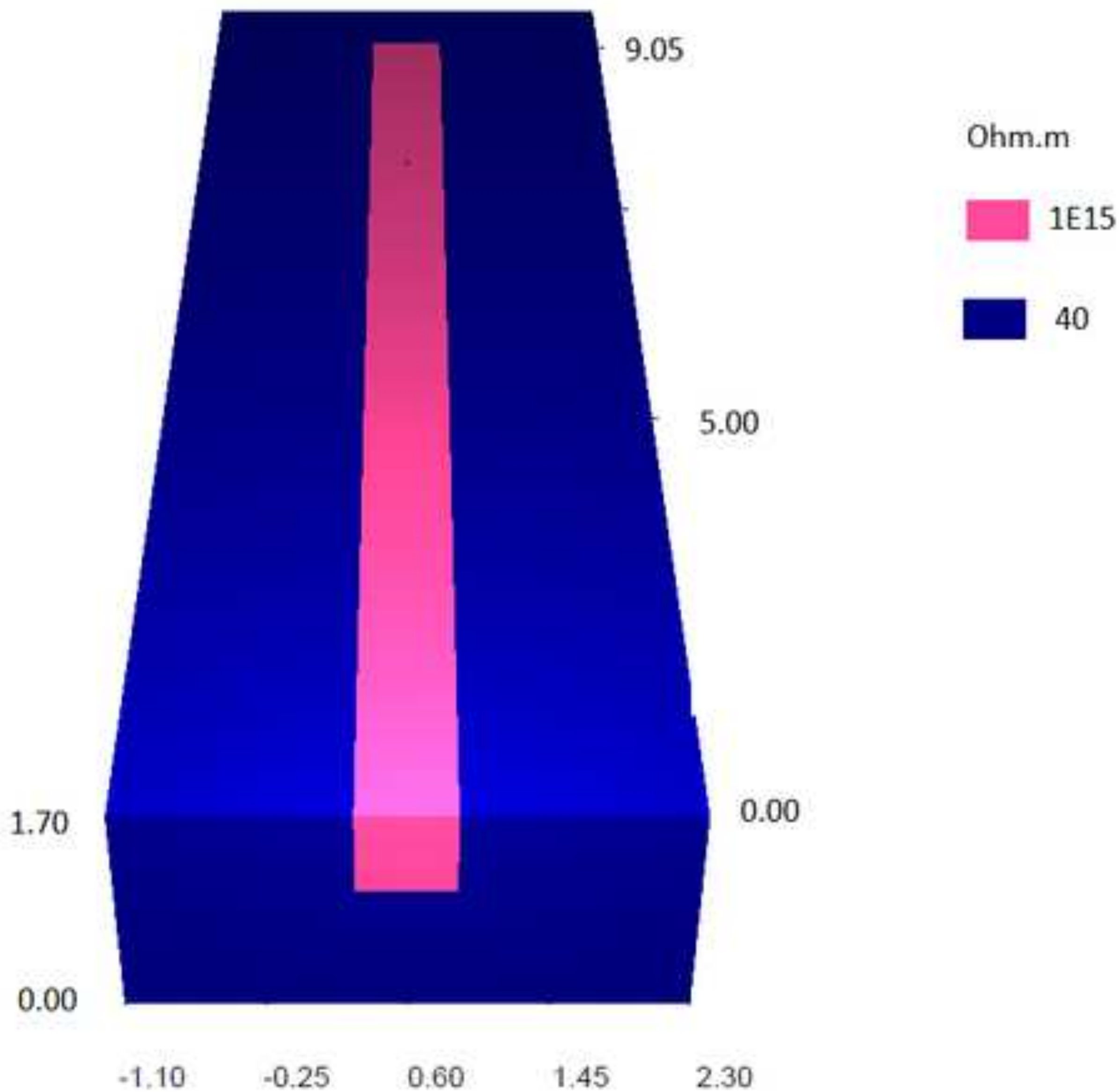
9.05
5.00
0.00
1.70
0.00
-1.10
-0.25
0.60
1.45
2.30
Ohm.m
1E15
40

Click here to download figure LOPES Figure14b.png

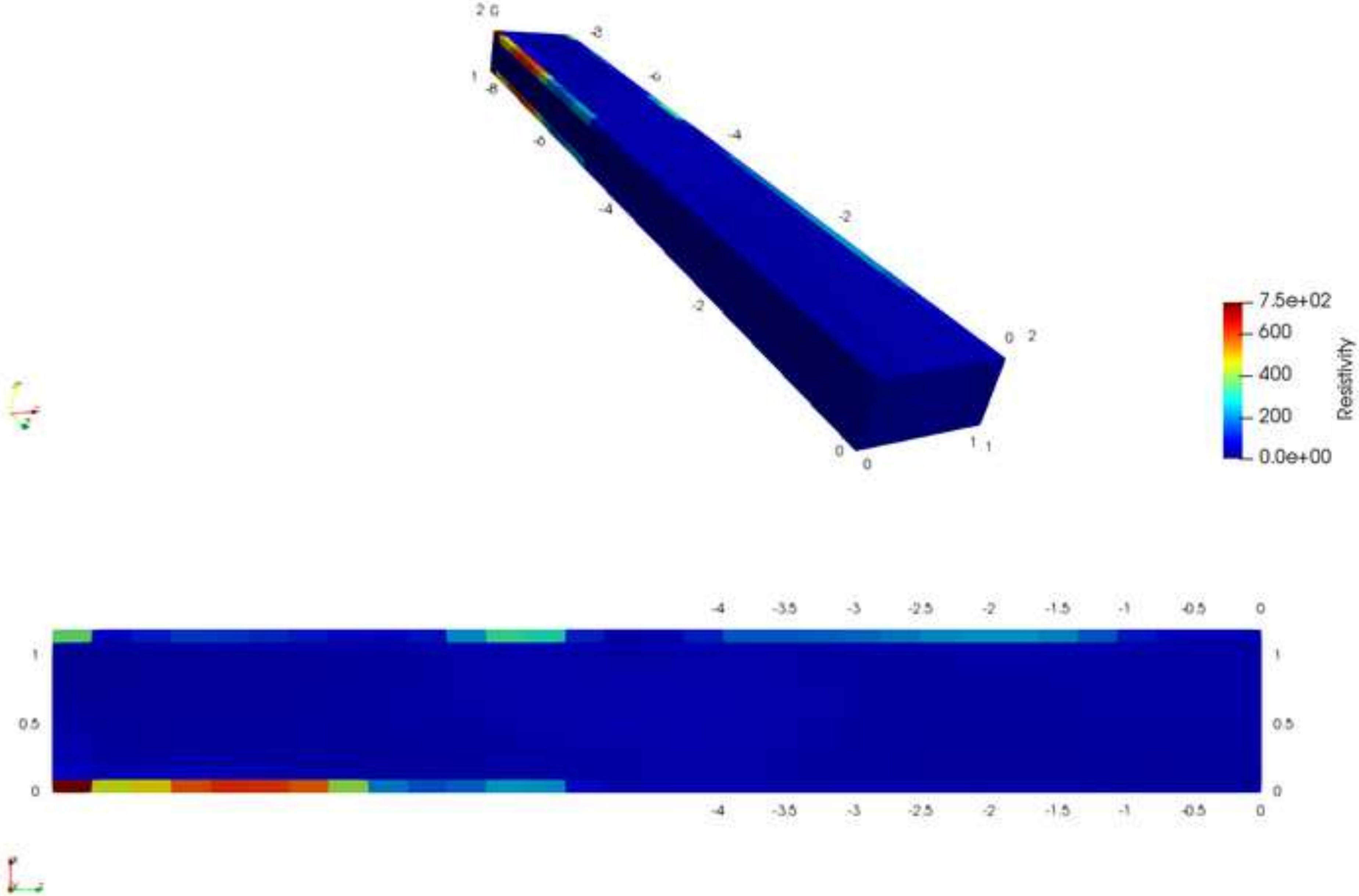

Click here to download figure LOPES Figure 1.pdf

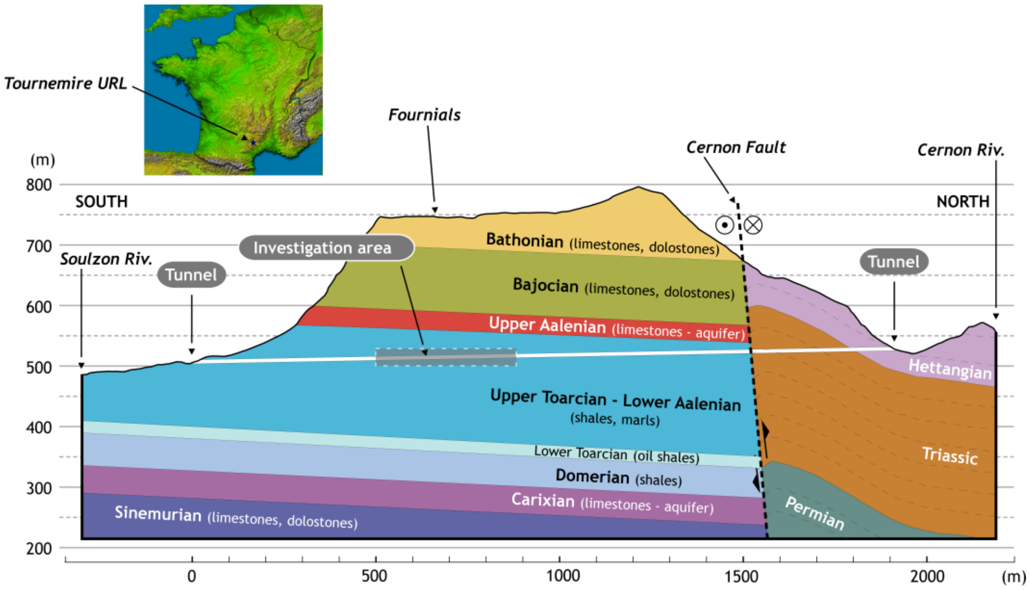

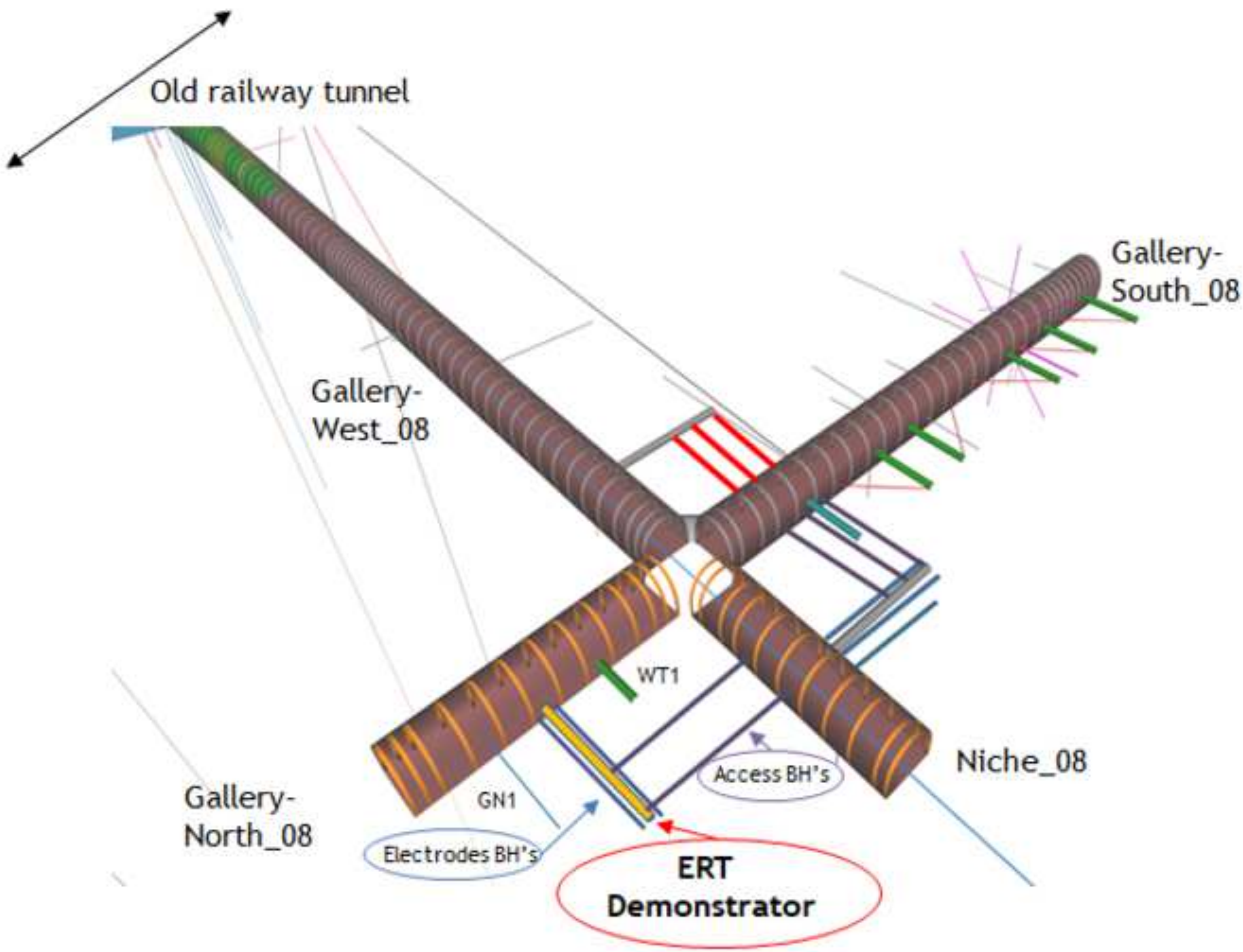
Old railway tunnel
Gallery-
South_08
Gallery-
West_08
WT1
Niche_08
Access BH's
Gallery-
North_08
GN1
Electrodes BH's
ERT
Demonstrator

Click here to download figure LOPES Figure 3.pdf

BLANK TEST 1 - January 2017

BLANK TEST 2 - January 2017

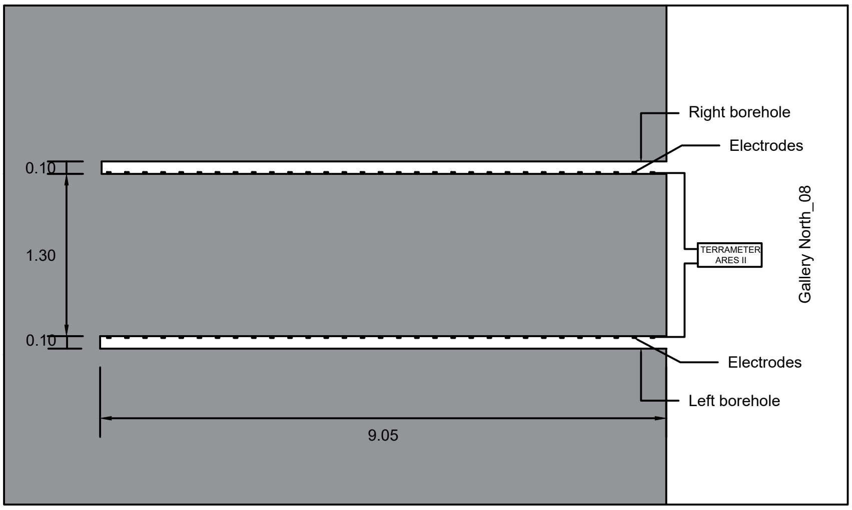

BLANK TEST 3 - November 2017

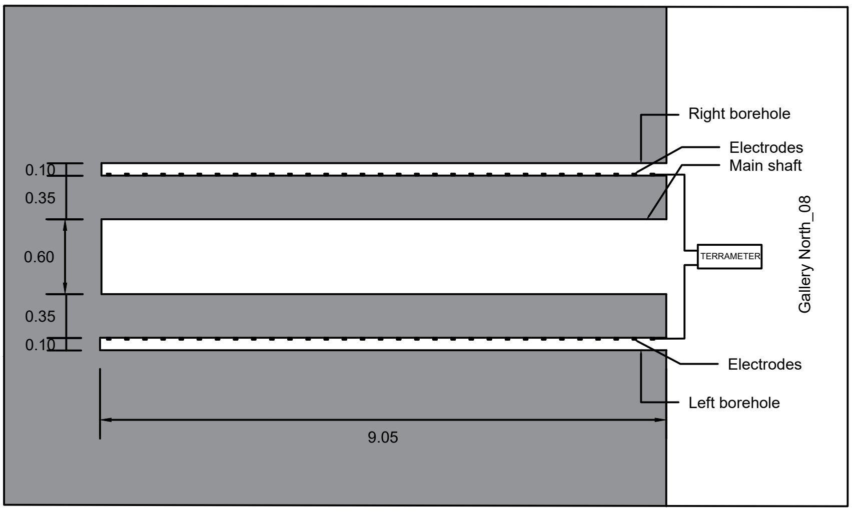

Click here to download figure LOPES Figure 4.pdf

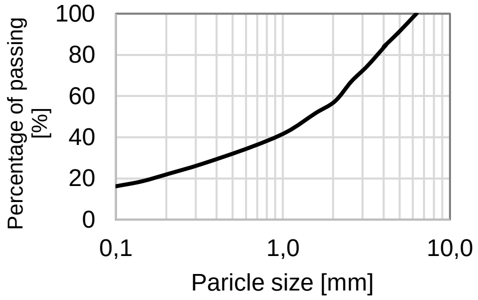

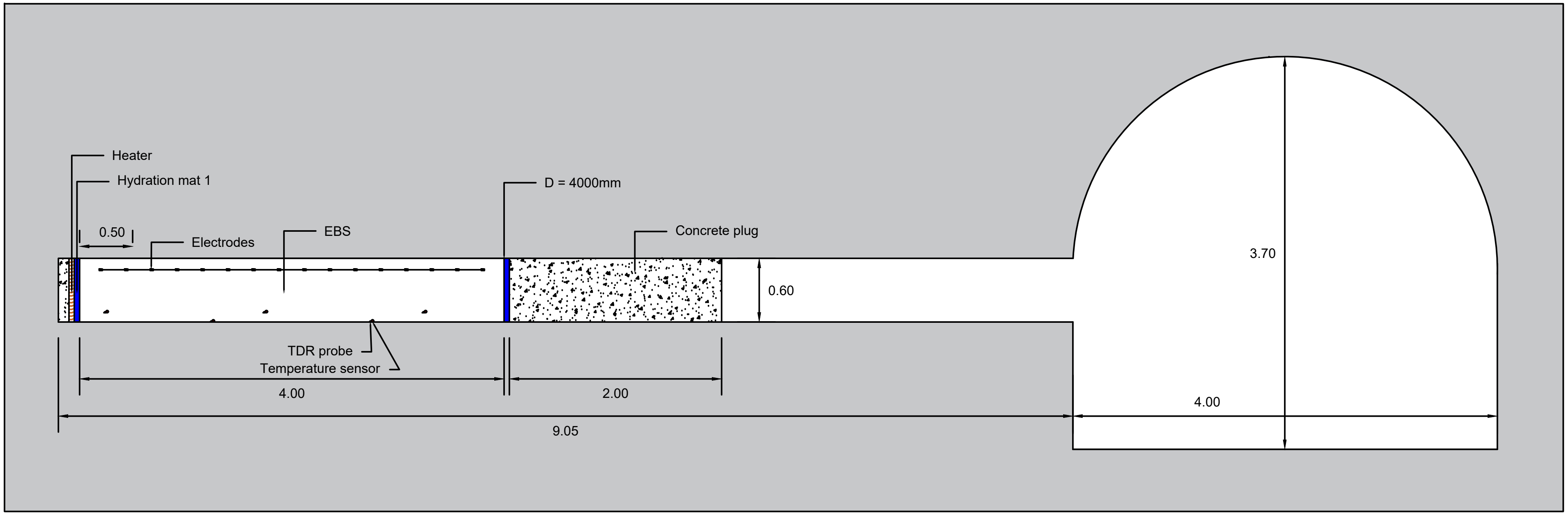
Heater
Hydration mat 1
D = 4000mm
0.50
Electrodes
EBS
Concrete plug
3.70
0.60
TDR probe
Temperature sensor
4.00
2.00
4.00
9.05

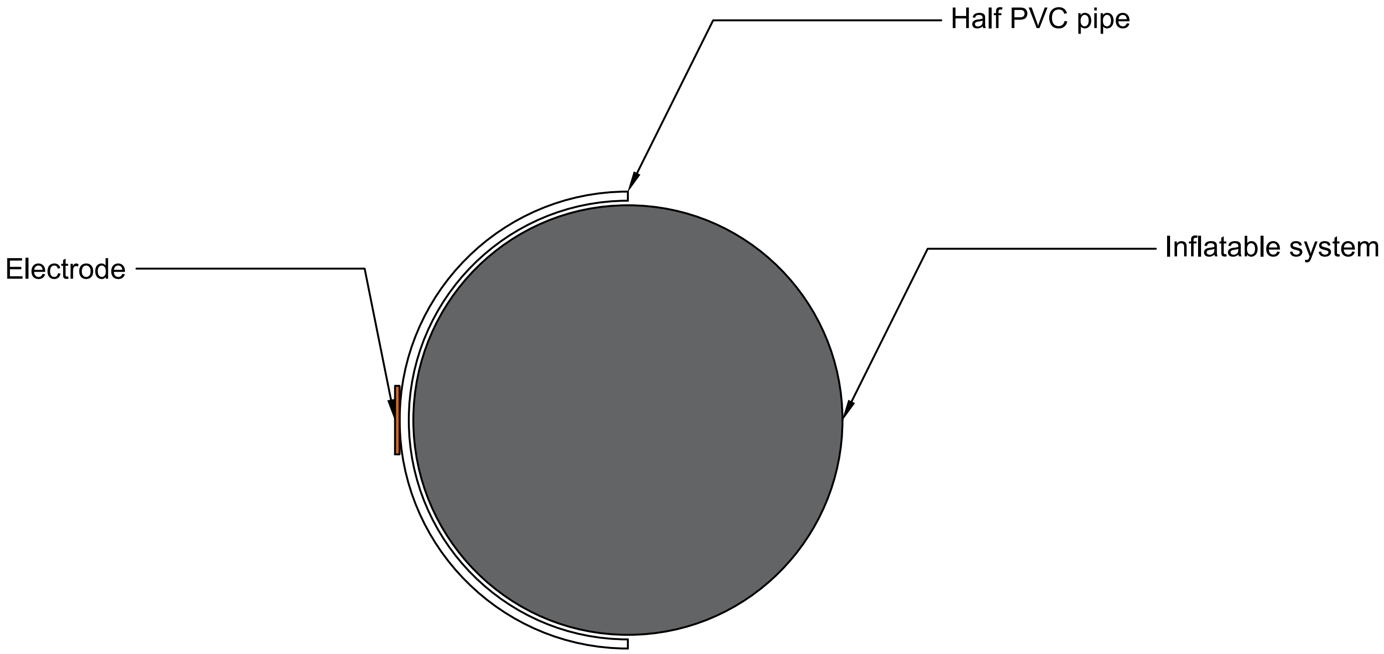
Half PVC pipe
Electrode
Inflatable system

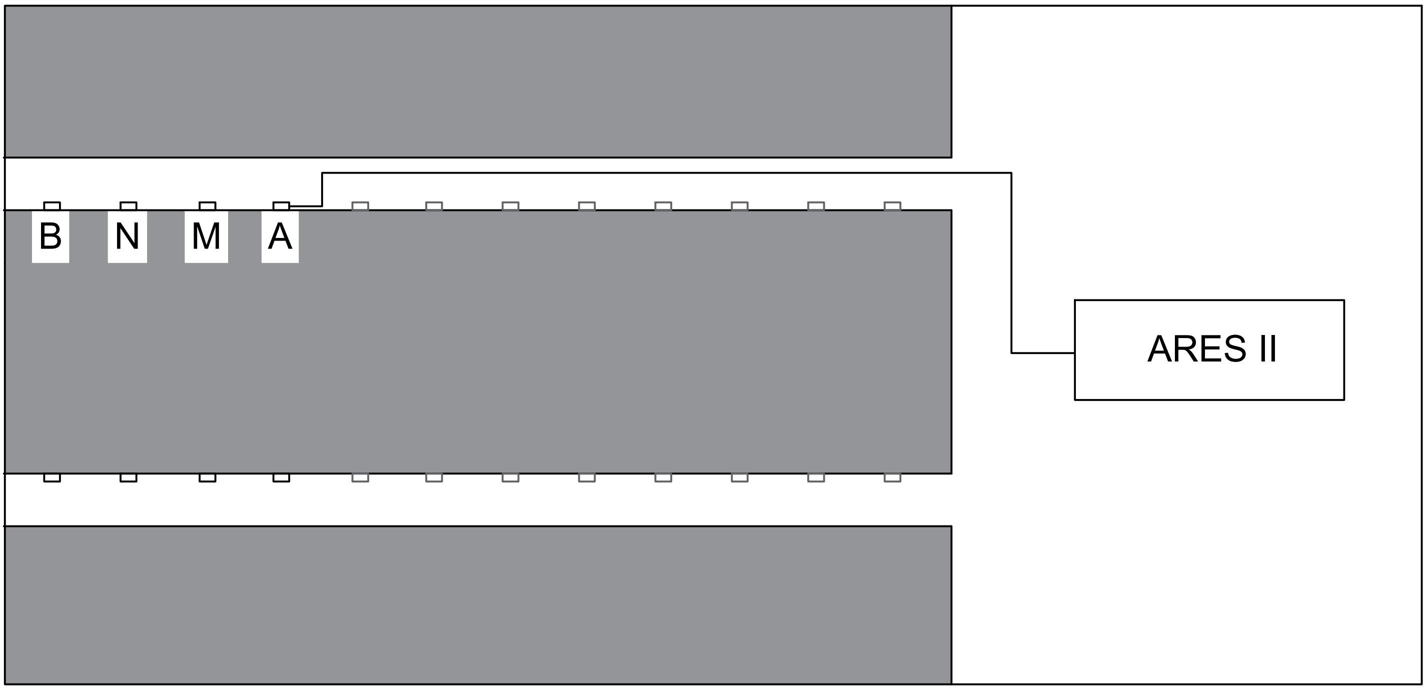
B
N
M
A
ARES II

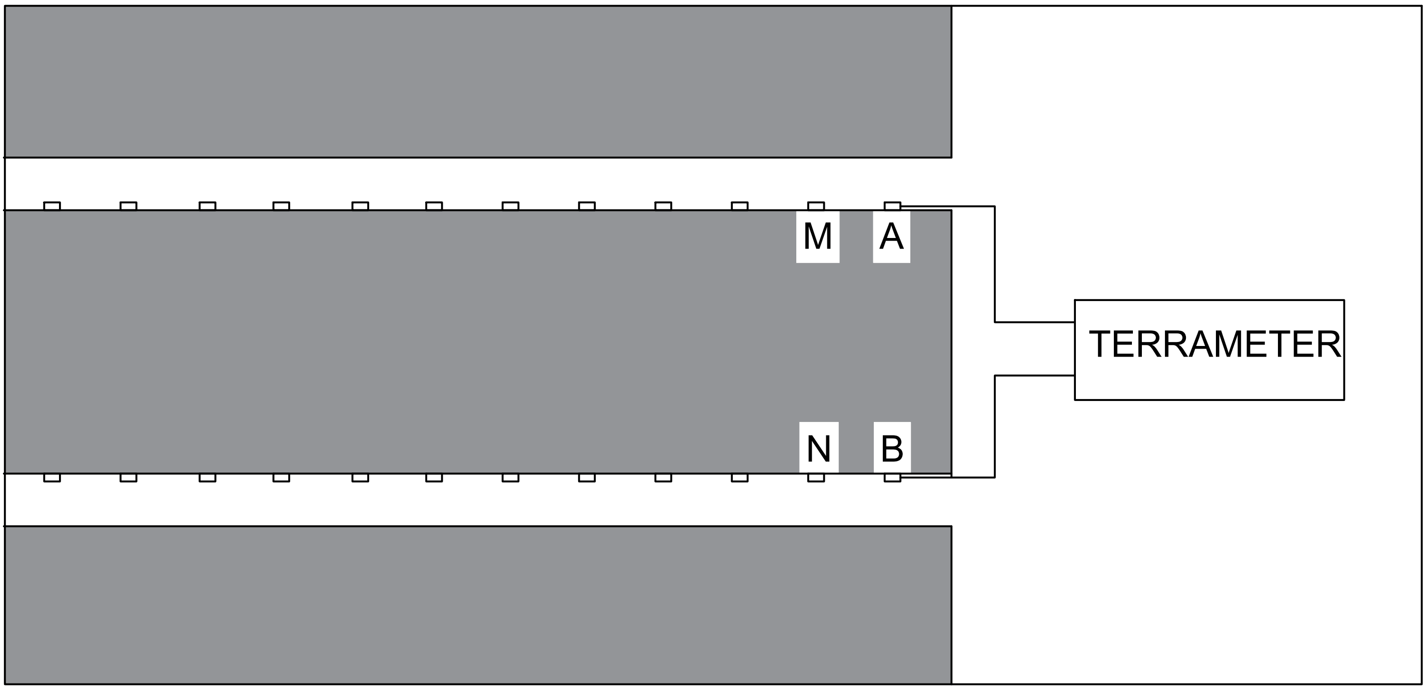
M
A
TERRAMETER
N
B

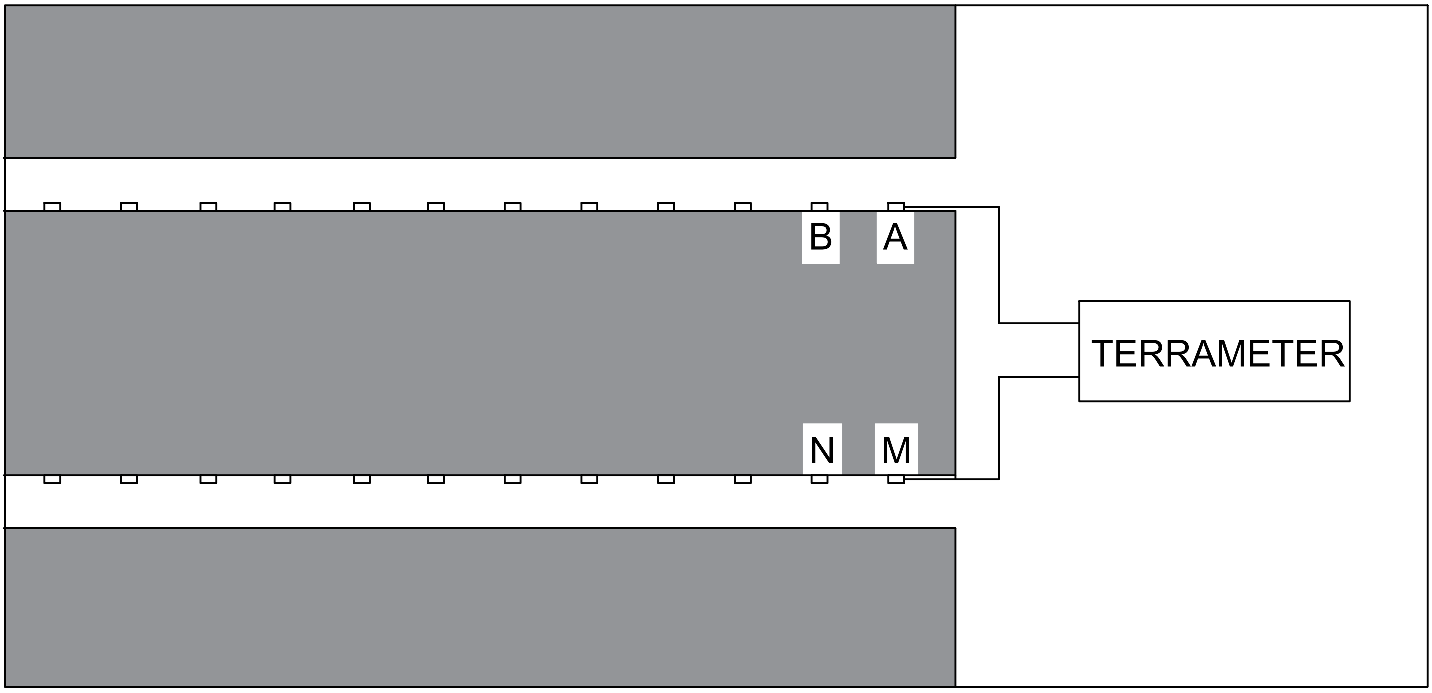
B
A
TERRAMETER
N
M

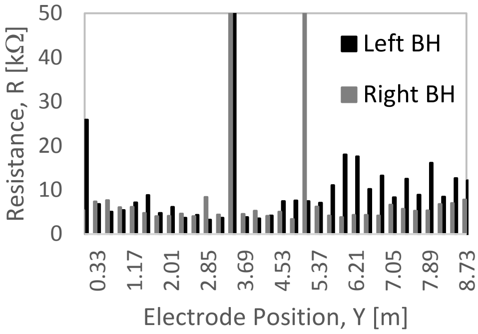

Resistance, R [kΩ]
50
40
30
20
10
0
Left BH
Right BH
0.33
1.17
2.01
2.85
3.69
4.53
5.37
6.21
7.05
7.89
8.73
Electrode Position, Y [m]

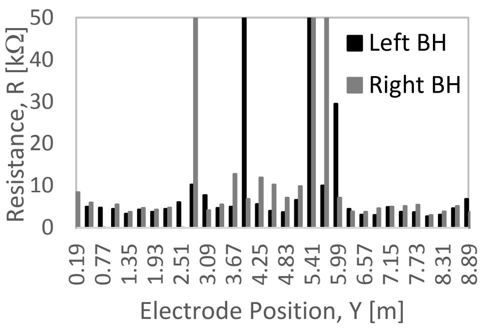

Resistance, R [kΩ]
50
40
30
20
10
0
Left BH
Right BH
0.19
0.77
1.35
1.93
2.51
3.09
3.67
4.25
4.83
5.41
5.99
6.57
7.15
7.73
8.31
8.89
Electrode Position, Y [m]

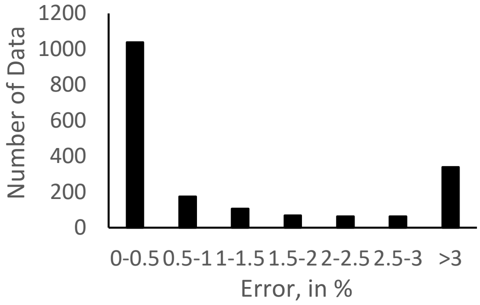
1200
1000
800
600
400
200
0
Number of Data
0-0.5
0.5-1
1-1.5
1.5-2
2-2.5
2.5-3
>3
Error, in %

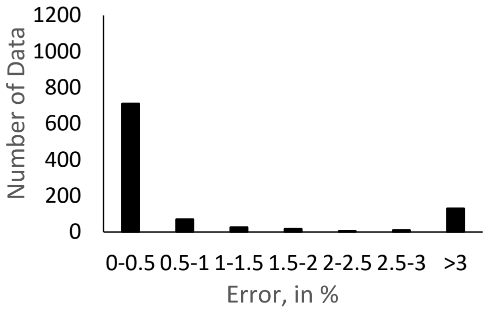
1200
1000
800
600
400
200
0
Number of Data
0-0.5
0.5-1
1-1.5
1.5-2
2-2.5
2.5-3
>3
Error, in %

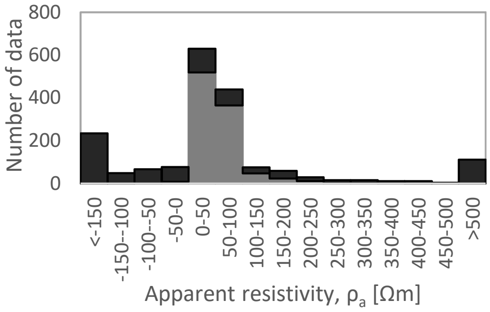
800
600
400
200
0
Number of data
<-150
-150--100
-100--50
-50-0
0-50
50-100
100-150
150-200
200-250
250-300
300-350
350-400
400-450
450-500
>500
Apparent resistivity, ρa [Ωm]